Computers and Concrete, *Vol. 22, No. 2 (2018) 167-182*
DOI: https://doi.org/10.12989/cac.2018.22.2.167

Finite element modeling of corroded RC beams using cohesive surface bonding approach

Mohammed A. Al-Osta[a], Hamdi A. Al-Sakkaf[b], Alfarabi M. Sharif[c], Shamsad Ahmad* and Mohammad H. Baluch[d]

Department of Civil & Environmental Engineering, King Fahd University of Petroleum & Minerals (KFUPM), Dhahran 31261, Saudi Arabia

(Received September 4, 2016, Revised May 30, 2018, Accepted June 1, 2018)

Abstract. The modeling of loss of bond between reinforcing bars (rebars) and concrete due to corrosion is useful in studying the behavior and prediction of residual load bearing capacity of corroded reinforced concrete (RC) members. In the present work, first the possibility of using different methods to simulate the rebars-concrete bonding, which is used in three-dimensional (3D) finite element (FE) modeling of corroded RC beams, was explored. The cohesive surface interaction method was found to be most suitable for simulating the bond between rebars and concrete. Secondly, using the cohesive surface interaction approach, the 3D FE modeling of the behavior of non-corroded and corroded RC beams was carried out in an ABAQUS environment. Experimental data, reported in literature, were used to validate the models. Then using the developed models, a parametric study was conducted to examine the effects of some parameters, such as degree and location of the corrosion, on the behavior and residual capacity of the corroded beams. The results obtained from the parametric analysis using the developed model showed that corrosion in top compression rebars has very small effect on the flexural behaviors of beams with small flexural reinforcement ratio that is less than the maximum ratio specified in ACI-318-14 (singly RC beam). In addition, the reduction of steel yield strength in tension reinforcement due to corrosion is the main source of reducing the load bearing capacity of corroded RC beams. The most critical corrosion-induced damage is the complete loss of bond between rebars and the concrete as it causes sudden failure and the beam acts as un-reinforced beam.

Keywords: reinforced concrete; reinforcement corrosion; modeling; finite-element analysis; bond slip; bond failure; residual capacity

1. Introduction

Corrosion of reinforcing steel bars (rebars) in reinforced concrete (RC) structures is the most serious durability concerns. Reinforcement corrosion causes various problems such as cracking and spalling of concrete cover, loss of the diameter and strength of rebars, and the loss of bond between rebars and the surrounding concrete that reduces the load carrying capacity of the reinforced concrete members. The loss of rebars-concrete bond due to reinforcement corrosion is one of the major factors, which affect the flexural behavior and load bearing capacity of the RC beams. Modeling of RC beams having corroded longitudinal reinforcing bars requires proper modeling for degradation in bond-slip behavior.

Eligehausen *et al*. (1983) proposed a segmental bond-slip behavior model based on the experimental data pertaining to the effects of different parameters. The bond-slip model given in FIB (2010) is based on the model of Eligehausen (1983). Steel-concrete interaction for non-corroded RC structures was studied by several researchers (Gan 2000, Soh *et al*. 1999, Wu and Zhao 2013). Almusallam *et al*. (1996), Lee *et al*. (2002) studied bond loss due to reinforcement corrosion experimentally using pullout tests. Mangat and Elgarf (1999), Stanish *et al*. (1999), Chung *et al*. (2004) examined the bond loss due to reinforcement corrosion in flexural members.

To simulate the rebars-concrete bond for modeling beams by finite element (FE) analysis, three different approaches have been reported in literature. First approach is to use the spring element to transfer the stress between rebar and concrete. This approach can be advantageously used with 2D modeling in which steel bars are modeled by two nodes truss elements and the nonlinearity of spring element can be prescribed by entering the experimental relationship of load versus displacement. The 1-D interface element, named translator in ABAQUS, was used by Li *et al*. (2014) to conduct numerical method to predict the behavior of corroded RC seawalls. The element has two nodes connecting the concrete and the steel bar, respectively, and actually represents the bond. Researchers

*Corresponding author, Professor
E-mail: shamsad@kfupm.edu.sa
[a]Assistant Professor
E-mail: malosta@kfupm.edu.sa
[b]MS Student
E-mail: g201206080@kfupm.edu.sa
[c]Professor
E-mail: fmsharif@kfupm.edu.sa
[d]Professor
E-mail: mhbaluch@kfupm.edu.sa

http://www.techno-press.org/?journal=cac&subpage=8
ISSN: 1598-8198 (Print), 1598-818X (Online)

such as Xiaoming and Hongqiang (2012) also used spring interface elements for bond modeling. Some other researchers used 4-noded interface elements to represent the bond in an ABAQUS environment (Val and Chernin 2009, Murcia-Delso and Shing 2015) and using DIANA software such as Kallias and Imran Rafiq (2010). The second approach is modeling the loss of bond between rebar and concrete by modifying concrete or steel properties. Ziari and Kianoush (2014) modified the material properties of concrete in contact with the reinforcing bar in small region, referred to as bond zone, to exemplify better bond interaction. In this zone, tensile strength and the fracture energy of the concrete elements are reduced. In the study conducted by Dehestani and Mousavi (2015), the bond interaction was considered by adding the equivalent strain of bond-slip effect to the strain of the steel bar. The third approach is to model the bond as an interaction between two 3D surfaces. This method can be used in ABAQUS software for 3D model of both concrete and steel. Amleh and Ghosh (2006) used this method for finite element pullout tests for corroded and non-corroded cases. Mechanical contact property was used in ABAQUS to describe the tangential and normal behavior between the contacting surfaces of concrete and steel.

Coronelli and Gambarova (2004), Kallias and Imran Rafiq (2010), Hanjari *et al*. (2011), Ou and Nguyen (2014) conducted two-dimension (2D) FE modeling for flexural-critical corroded beams using interface elements to simulate the rebars-concrete bond. Damage for concrete and steel elements due to corrosion was introduced by suitable reduction of their non-corroded properties according to available models or by removal of spalled concrete. Sánchez *et al*. (2010) presented a 2D finite element model (FEM) to simulate corroded RC members using Continuum Strong Discontinuity Approach (CSDA) to model the concrete. The concrete-steel interface is modeled by using contact-friction elements with the friction loss as a function of the degree of corrosion.

Biondini and Vergani (2014), Almassri *et al*. (2016) conducted 3D FEM for corroded beams without considering the bond loss. Xiaoming and Hongqiang (2012) conducted 3D FEM in ANSYS, considering the bond being modeled by interface elements of type Combin39. However, no validation with experimental work was presented. German and Pamin (2015) in their nonlinear FEM modeling in ABAQUS carried out a 2D and 3D FE modeling for corroded beams with corrosion product (rust) being modeled as interface element (COH2D4 elements) in ABAQUS. Potisuk *et al*. (2011), Bernard (2013), Almassri *et al*. (2015) conducted FEM of corroded shear-critical beams.

From the literature review as presented above, it is found that very little 3D FEM works are done for corroded RC beams especially considering bond loss in the modeling. Further, there is lack of 3D FEM of corroded RC beams, which would enable the researchers to study the behaviour of RC beams in a more general way. For example, examining the effect of corrosion that happens only on the exterior face of the beam or at one corner of the beam. In this study, modelling of RC beams via 3D nonlinear FE analysis in ABAQUS software was conducted for both non-corroded and corroded beams that exhibited different failure modes (shear, flexural, and bond). In addition, a parametric study was conducted to examine the effects of some damage parameters due to corrosion for instance, degree and location of the corrosion on the behaviour and residual strength of the corroded RC beams.

2. Research methodology

2.1 Bond simulation based on surface interaction in ABAQUS

Unlike FE modeling for non-corroded beams, perfect bond assumption is not applicable for beams that have corroded reinforcements. Therefore, this study aims to get benefit from the 3D surface interaction modeling techniques available in ABAQUS to simulate bond for corroded and non-corroded RC beams.

Two main approaches reported in literature to simulate the bond can be used in ABAQUS for the rebar-concrete surface interaction. The first approach is surface-based mechanical contact in which the behavior of the contact (contact property) is defined in two directions: normal and tangential to the contacting surfaces. A pure master-slave contact algorithm is used in ABAQUS considering that nodes on one surface (the slave) cannot penetrate the segments that make up the other surface (the master). In the case of RC, the slave surface is the rebar and the master surface is the concrete (Amleh and Ghosh 2006). Mechanical contact approach can be further classified to many methods according to different properties that have to be input for normal or tangential direction such as friction and the pressure. The second main approach is surface-based cohesive behavior which is a mechanical model based on traction-separation behavior. This cohesive behavior allows the bond between two surfaces to be expressed as a linear elastic relationship between traction (t) and separation or slip (δ). Some researchers used this approach in 2D modeling of pull-out tests such as Wenkenbach (2011) who studied the tension stiffening in RC members with large diameter rebars. Henriques *et al*. (2013) used surface-based cohesive behavior in 3D modeling of beam but without considering bond loss.

2.1.1 Surface-based mechanical contact approach

As mentioned earlier, the surface-based mechanical contact depends on both normal and tangential behaviors that should be considered to define a full contact property between concrete and steel or RC beam. In the surface based contact approach, shear and normal forces are transmitted across the interface of surfaces as they are in contact. The normal and tangential behaviors of the surface based contact between rebars and concrete are described in the following sub-sections.

2.1.1.1 Normal behavior of surface based contact

The normal behavior of the contact property can be defined by pressure-overclosure relationships. The default pressure-overclosure contact in ABAQUS is called “hard” contact. In this behavior, the contact constraint in direction

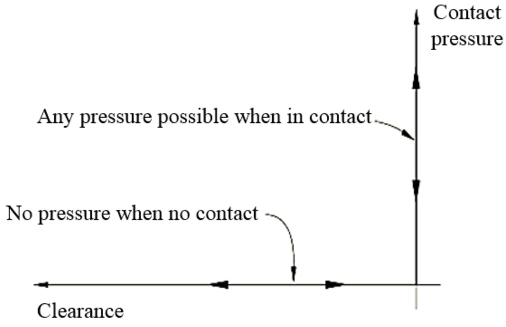

Fig. 1 Contact pressure-clearance relationship for "hard" contact (Simulia 2013)

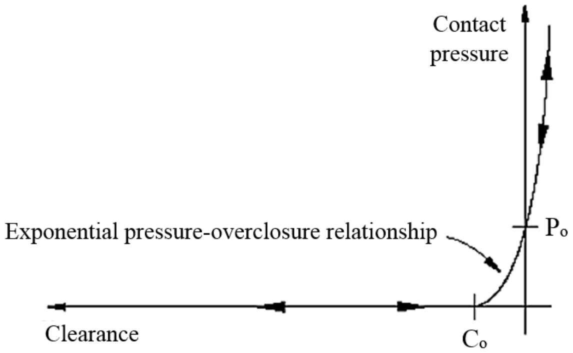

Fig. 2 "Softened" exponential pressure-overclosure relationship (Simulia 2013)

normal to the contacting surfaces, is applied when the distance separating two surfaces, called clearance, becomes zero and there is no limit on the value of contact pressure that can be passed on between the surfaces. When the contact pressure between the surfaces becomes zero or negative, the surfaces separate, and the constraint is removed and the transfer of tensile stress in normal direction across the interface is not allowed (Fig. 1).

Other available types for pressure-overclosure behavior include using a linear law, a tabular piecewise-linear law, or an exponential law. Linear pressure-overclosure can be defined by specifying the contact stiffness in (N/mm^2/mm). The exponential law, as shown in Fig. 2, is found to be the optimal to model corrosion (Amleh and Ghosh 2006). When the surfaces get closer, this relationship takes into consideration the increase in pressure, and allows the pressure to become zero if the surfaces are no longer in contact. Using the results from pull out tests presented by Amleh and Ghosh (2006), the pressure at zero clearance (P_0) for non-corroded case was related to the concrete cover thickness (C) by Eq. (1)

$$P_0 = 0.128C + 1.5 \tag{1}$$

where: P_0 is in MPa and C is in mm.

2.1.1.2 Tangential behavior of surface based contact

The tangential behavior can be expressed in terms of the frictional forces that resist the relative sliding of the surfaces. The common Coulomb's friction model that describes the friction between the surfaces can be used to describe the tangential behavior. The value of critical shear

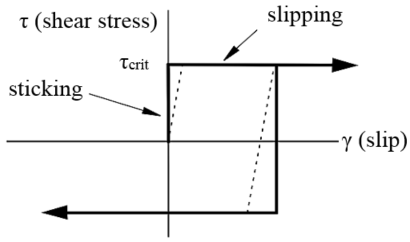

Fig. 3 Penalty friction formulation behavior (Simulia 2013)

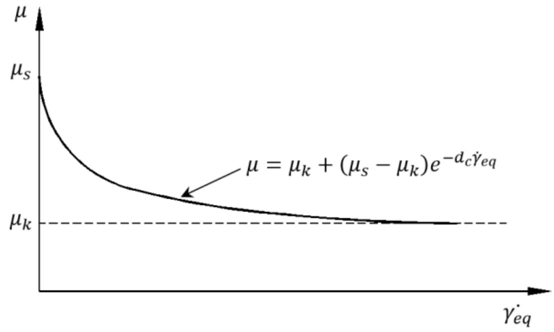

Fig. 4 Exponential decay friction model (Simulia 2013)

stress (τ_{crit}) can be given by the following equation in term of the normal contact pressure (P)

$$\tau_{\text{crit}} = \mu P \tag{2}$$

The value of coefficient of friction, μ, is assumed to be same in all the directions (isotropic friction).When the surface traction reaches a critical shear stress value, the tangential motion is not equal to zero.

The ideal behavior of friction is very complicated to simulate. Hence, in many cases, ABAQUS uses a penalty friction formulation with an allowable "elastic slip," shown by the dotted line in Fig. 3. The penalty stiffness (the slope of the dotted line) is automatically chosen in ABAQUS so that the allowable "elastic slip" is a very small fraction of the characteristic element length (Simulia 2013).

In ABAQUS, an exponential decay law (Fig. 4) is used to model the transition between static and kinetic friction. In this model, the friction coefficient decays exponentially according to following formula:

$$\mu = \mu_k + (\mu_s - \mu_k)e^{-d_c \dot{\gamma}_{\text{eq}}} \tag{3}$$

where: μ_s=static friction coefficient, μ_k =kinetic friction coefficient, d_c is a user-defined decay coefficient, and $\dot{\gamma}_{\text{eq}}$ =slip rate.

Following three different methods, based on the principle of surface-based mechanical contact, were examined:

1) Method-1: Contact property in which the tangential behavior is defined by a penalty friction formulation, using constant friction coefficient=1 and no shear limit was used in this study, as initial FE modeling shows no effect. The normal behavior is defined by using a "hard" contact relationship.

2) Method-2: Contact property in which the normal behavior is linear pressure-overclosure defined by contact stiffness=1000 N/mm^2/mm, as suggested by German and

Pamin (2015). The tangential behavior is the same as method-1 (i.e., penalty friction with coefficient=1)

3) Method-3: Contact property with tangential behavior defined by exponential decay friction model and normal behavior defined by softened contact with an exponential pressure overclosure relationship. The parameters used for this third method were according to Amleh and Ghosh (2006).

2.1.2 Surface-based cohesive behavior approach

In this approach, the bond between two surfaces is expressed as a linear elastic relationship between traction (t) (bond stress) and separation (δ) (slip). Typically, ABAQUS has two methods for simulating the bonded interface behavior using traction-separation behavior. One is cohesive elements, and another is surface-based cohesive behavior. In this study, the thickness of the interface is negligible. Consequently, surface-based cohesive method is used due to its convenience and effectiveness. The traction-separation model consists of two parts in ABAQUS, which includes the initial linear elastic behavior and the post-elastic behavior that is identified by the initiation and evolution of bond damage. An elastic constitutive matrix represents the elastic behavior, which relates the shear and normal stresses to the shear and normal separations across the interface (ABAQUS Manual 2013).

The constitutive relation for initial elastic part can be uncoupled or coupled, as expressed in Eqs. (4) and (5), respectively.

$$t=\begin{pmatrix}t_n\\t_s\\t_t\end{pmatrix}=\begin{pmatrix}K_{\mathrm{nn}}&0&0\\0&K_{\mathrm{ss}}&0\\0&0&K_{\mathrm{tt}}\end{pmatrix}\begin{pmatrix}\delta_n\\\delta_s\\\delta_t\end{pmatrix}=\mathrm{K}\delta \tag{4}$$

$$t=\begin{pmatrix}t_n\\t_s\\t_t\end{pmatrix}=\begin{pmatrix}K_{nn}&K_{ns}&K_{nt}\\K_{ns}&K_{ss}&K_{st}\\K_{nt}&K_{st}&K_{tt}\end{pmatrix}\begin{pmatrix}\delta_n\\\delta_s\\\delta_t\end{pmatrix}=K\delta \tag{5}$$

In the present work, since the uncoupled behavior is used as suggested by many researchers, the values of stiffness K_{nn}, K_{ss}, and K_{tt}, have to be defined. The unit of the constants in the K stiffness matrix is [Force/Length^2/ Length]. These stiffness elements, which define the contact in normal and tangential directions, can be determined based on exponential decay.

The post-elastic behavior, which can be identified by the initiation and evolution of bond damage, can be modeled using the relationship between the bond stress and slip of steel bar. This relationship can be approximated by using the bond damage criterion where the damage initiates as soon as any one of the three separation or slip models (Eq. (6)) is triggered when corresponding stress exceeds a maximum allowable value. This criterion can be represented as

$$Max\left\{\frac{<t_n>}{t_n^0},\frac{t_s}{t_s^0},\frac{t_t}{t_t^0}\right\}=1 \tag{6}$$

The normal stress, t_n, in Eq. (6) is kept within Macaulay brackets. This is to avoid a compressive stress (t_n < 0) resulting in damage initiation.

Damage evolution describes the way in which the interface stiffness degrades once the damage initiation criterion is met. In ABAQUS, there is a choice for a linear, exponential, or user defined response for this cohesive damage evolution. Linear response is defined by specifying the maximum effective separation (δ_m) at which the bond is fully degraded. It is given as

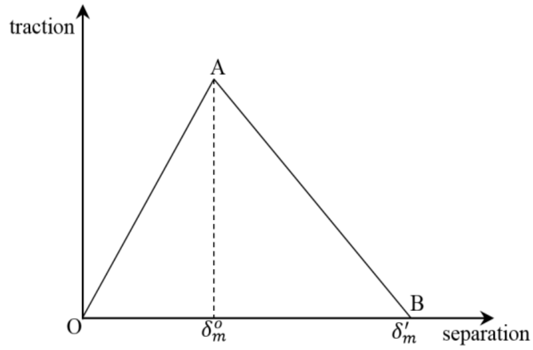

Fig. 5 Bond traction separation characteristic with linear damage evolution

$$\delta_m=\sqrt{<\delta_n>^2+{\delta_s}^2+{\delta_t}^2} \tag{7}$$

In this study, linear damage evolution is used by specifying δ_m=maximum slip in longitudinal tangential direction because slip values in the other two directions are very small compared to it. This damage evolution was chosen because it is simple and accurate. This is evident from the small difference in results of four different cohesive damage models in ABAQUS, reported by Wenkenbach (2011). Fig. 5 shows the full bond behavior characteristic. The damage initiation starts at point *A* and damage evolution describes the behavior from point *A* to point *B*.

To make the maximum shear stress control the behavior, large value for maximum t_n should be used. The maximum bond strength ($t_{\max}$) is represented in ABAQUS by t_s and that t_t has no effect on behavior since there is almost no stress in transverse direction of the bar.

2.2 Modeling of non-corroded beam

Finite element model for non-corroded RC beams was constructed first using simple perfect bond method in which steel and concrete elements are tied by their connecting interface nodes. Subsequently, the FE models were developed considering all contact methods for simulating the rebar-concrete bond described earlier. Using the experimental data reported in literature, comparison of FE model based on the perfect bond criteria with that based on the contact methods was carried out to select the most accurate approach.

2.2.1 Finite element modeling

ABAQUS, one of the most widely used and available software packages, was used for finite element modeling (FEM). Three-dimensional 8-noded linear brick element (C3D8R) for both concrete and longitudinal reinforcement bars and two-nodded element (T3D2: A 2-nodded linear 3-D truss element type) for the stirrups were considered (Fig.

Table 1 Parameters used for CDP model

Dilatation angle ψ	Flow potential eccentricity ε	Initial biaxial compressive stress to initial compressive stress f_{b0}/f_{c0}	Ratio of second stress invariant on the tensile meridian K_c	viscosity parameter λ
36	0.1	1.16	0.67	0

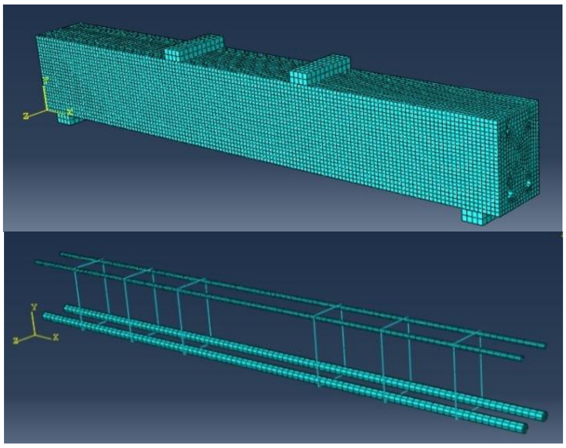

Fig. 6 3D FE model for beam in ABAQUS

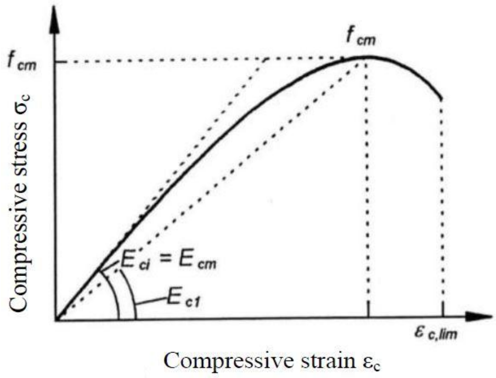

Fig. 7 Schematic representation of the stress-strain relation for uniaxial compression (FIB 2010)

6). The steel plates at supports and loading points were used in the model to prevent any stress concentration and ensure uniform pressure to the top surface of steel loading plates. These plates were also modelled by using C3D8R elements. The bond between the plates and concrete is considered as Tie (perfect) bond. The bond between the both concrete and longitudinal reinforcement bars was modelled by different methods as mentioned above.

The type of analysis used was "Dynamic Explicit". Dynamic Explicit can be used to simulate material degradation or failure, such as cracking of concrete. This type of analysis was chosen based on the fact that this method is powerful in solving problems that are static such as Quasi-static process simulation problems involving complex contact (Simulia 2013). From many previous researchers, analysis using this method rarely encounters any problems of convergence. This solution technique is a direct-integration dynamic procedure that uses the central-difference operator to march in pseudo-time (Ziari and Kianoush 2014). However, it should be noted that using dynamic analysis for static problems, inertial effects should be reduced by using slow loading rates or by increasing the mass density so that the oscillation of the results is limited (Mercan 2011).

2.2.1.1 Concrete behavior model

Three different techniques for modeling nonlinear behavior of concrete are available in ABAQUS: the Smeared Cracking Model (SC), the Concrete Damaged Plasticity model (CDP), and the Brittle Cracking model. The CDP was used in this study because it is more stable for the numerical computations, especially in failures that exhibit a softening bias. This CDP was developed by Lubliner *et al*. (1989) and extended by Lee and Fenves (1998). It requires the values of elastic modulus, Poisson's ratio, the description of compressive and tensile stress-plastic strain behavior, and five plastic damage parameters, as illustrated in Table 1. Dilatation angle used was 36^o, which is commonly assumed for concrete. For the remaining four parameters, default values are used as suggested by ABAQUS (Table 1).

The hardening and softening in compression of the concrete was implemented in ABAQUS based on CEB-FIP Model Code (2010), as shown in Fig. 7, and expressed by Eqs. (8) through (10). The linear part of compression curve was assumed up to 0.4 $f_c^{'}$. The CDP model requires this data in the form of stress-inelastic strain.

$$\frac{\sigma_c}{f_{\mathrm{cm}}} = \frac{\mathrm{k}\eta - \eta^2}{1 + \eta(k-2)} \tag{8}$$

where: σ_c =concrete stress, f_{cm} =mean concrete cylinder compressive strength, k and η are two factors determined according to Eqs. (9) and (10), E_{c1} is the secant modulus of elasticity of concrete from origin to peak compressive stress, ε_c is the concrete strain, ε_{c1}=compressive strain at f_{cm}.

$$\eta = \frac{\varepsilon_c}{\varepsilon_{c1}} \tag{9}$$

$$k = \frac{E}{E_{c1}} \tag{10}$$

The behavior of concrete in tension is assumed as linear elastic until concrete cracking is started at a modulus of rupture of concrete, f_t, that can be estimated by Eq. (11) based on the ACI-318-14. After cracking, linear softening part is used with $W_c=2G_f/f_t$ as shown in Fig. 8 after converting the cracking opening to strain values by dividing it by a characteristic length, l_c, (for concrete it is assumed equal to three times the maximum aggregate size) (Bossio *et al*. 2015)

$$f_r = 0.62\sqrt{f_c^{'}} \tag{11}$$

The fracture energy G_f is calculated by the following expression

$$G_F = 73(f_t)^{0.18} \tag{12}$$

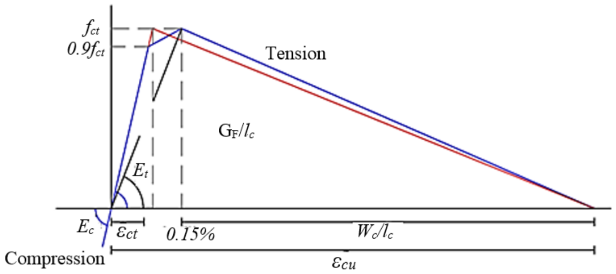

Fig. 8 Bilinear concrete tension model (Bossio *et al*. 2015)

The CDP model required the data for the compression and tension damage parameters (d_c and d_t). These parameters can be estimated from Eqs. (13) and (14) given by Birtel and Mark (2006), with b_c and b_t values between 0 and 1.

$$d_c = 1 - \frac{\sigma_c E^{-1}}{\varepsilon_c^{\mathrm{pl}}(1/b_c - 1) + \sigma_c E^{-1}} \tag{13}$$

$$d_t = 1 - \frac{\sigma_t E^{-1}}{\varepsilon_t^{\mathrm{pl}}(1/b_t - 1) + \sigma_t E^{-1}} \tag{14}$$

2.2.1.2 Steel behavior model

An elasto-plastic behavior with hardening was considered. The stress-strain curve for the non-corroded rebar was established according to stress-strain model given by Mander (1983). Linear-isotropic behavior was used for steel plates. The modulus of elasticity, E_s, and the Poisson's ratio, v, of steel rebars and steel plates were considered as 200000 N/mm^2 and 0.3, respectively.

3. Experimental data considered for validation of FE models

3.1 Lachemi et al. (2014)

The experimental data pertaining to the shear behavior obtained by testing the beam specimens, as reported by Lachemi *et al*. (2014), was considered for validation of the results of the FE models for non-corroded and corroded beams. Lachemi *et al*. (2014) experimentally examined shear behavior of corroded beams made of normal concrete (NC). The 28-day compressive and splitting tensile strengths of concrete were 45.5 MPa and 5.2 MPa, respectively. The yield strengths of longitudinal steel and strirrups were taken as 550 MPa and 400 MPa, respectively. The beams were subjected to four levels of reinforcement corrosion to induce mass losses of 5, 10, 15, and 20% in both shear stirrups and bottom rebars. Dimensions of the tested beams were 150 mm×220 mm×1400 mm and shear span ratio, *a/d*, was 2.5, as shown in Fig. 9. This experimental data considered for validation of the models belonged to three different beam specimens NC-B2, NC-B4, and NC-B7 (Table 2), as designated by Lachemi *et al*. (2014). The beam specimen (NC-B2) had a small shear span length of 440 mm over which the reinforcement needs to be developed with no end hooks. Therefore, it was considered critical for bond strength.

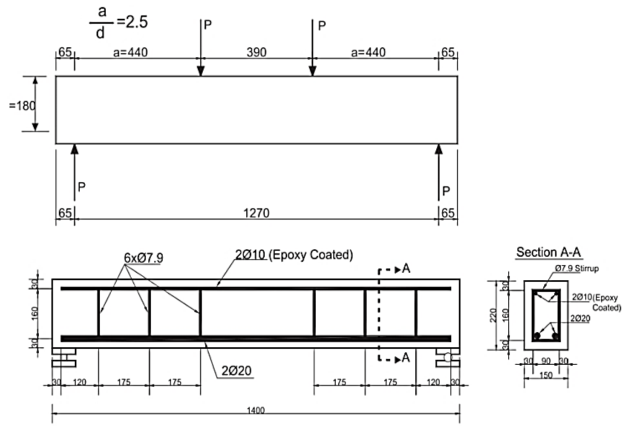

Fig. 9 Beam used for bond modelling methods (Lachemi *et al*. 2014) (all dimensions in mm)

Table 2 Properties of beams tested by Lachemi *et al*. (2014)

Beam Specimens	Average corrosion mass loss (X_p) %		f_c' (MPa)
	Tension bars	Stirrups	
NC-B2	(0.0) control beam (un-corroded)		45.5
NC-B4	14.62		45.5
NC-B7	10.61		45.5

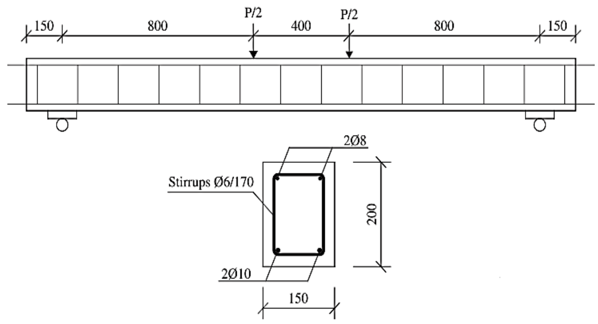

Fig. 10 Beams tested by Rodriguez *et al*. (1996) (all dimensions are in mm)

3.2 Rodriguez et al. (1996)

The experimental data reported by Rodriguez *et al*. (1996) by testing non-corroded and corroded RC beam specimens in flexure were utilized to validate the proposed method of cohesive interaction of bond modeling. The details of beam specimens are shown in Fig. 10. The concrete used for casting different beam specimens had various compressive strengths, as follows: 50 MPa for B-111 and 34 MPa for B-113 and B-115. The yield strength of the 10-mm rebars used was 575 MPa. The corrosion induced in beams B-113 and B-115 resulted into different mass losses of tension and compression rebars and stirrups, as shown in Table 3.

3.3 Du et al. (2007)

The experimental data reported by Du *et al*. (2007) obtained by testing a partially corroded beam (designated as

Table 3 Properties of beams tested by Rodriguez *et al*. (1996)

Beam Spec.	Corrosion mass loss (X_p) %			f_c' (MPa)
	Tension bars	Compression bars	Stirrups	
B111	(0.0) control beam (un-corroded)			50
B113	18.64	26.04	30	34
B115	13.9	12.58	23.15	34

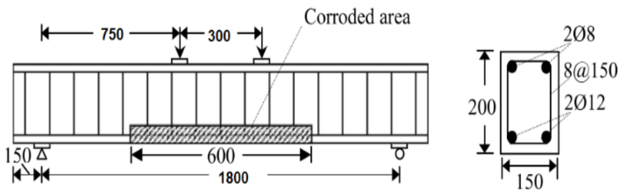

Fig. 11 Dimensions (in mm) and reinforcement details for the corroded beam T282 (Du *et al*. 2007)

Table 4 The properties of steel bars used in beam T282 (Du *et al*. 2007)

Steel Properties	Bar diameter	
	8 mm	12 mm
Yield strength (f_y), MPa	526	489
Ultimate Strength (f_u), MPa	619	595
Elasticity (E_s), MPa	200000	
Hardening Strain (ε_{sh})	0.022	0.02
Ultimate strain (ε_{uo})	0.082	0.132

T282) was utilized for validation of the models for flexural behavior of partially corroded RC beams. The bottom bars of the beam were corroded with a mass loss of 11.1% over a length of 600 mm of the beam's span, as shown in Fig. 11. The beam was made of concrete with a compressive strength of 44.5 MPa. The properties of steel rebars used in the beam are shown in Table 4.

4. Results and discussion

4.1 Validation of models for non-corroded beam

4.1.1 Perfect bond case

The load-deflection data pertaining to beam NC-B2, reported by Lachemi *et al*. (2014), was used to validate the proposed FE model for non-corroded beams based on perfect bond between rebars and concrete. Fig. 12 shows the load-deflection curves obtained from the FE model and the selected experimental data. It can be observed that there is a good agreement between the both load-deflection curves, which is expected for non-corroded beams because the perfect bond assumption is reported to be accurate for non-corroded beams. However, modeling for corroded beams using perfect bond method cannot be appropriate because of inability to account for the loss of bond due to reinforcement corrosion.

Since the FE model developed for perfect bond case is validated using experimental data, the load-deflection data obtained from this model were used as benchmark for

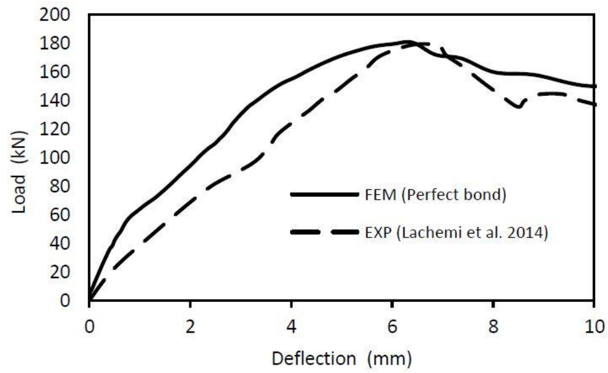

Fig. 12 Load-deflection curve validation for perfect bond method for beam NC-B2

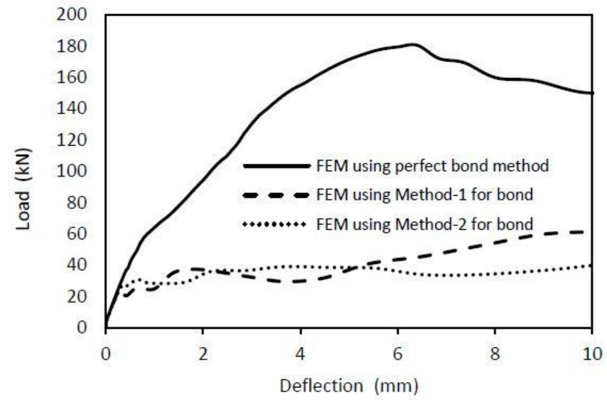

Fig. 13 Results of contact modeling using Methods 1and 2 for NC-B2

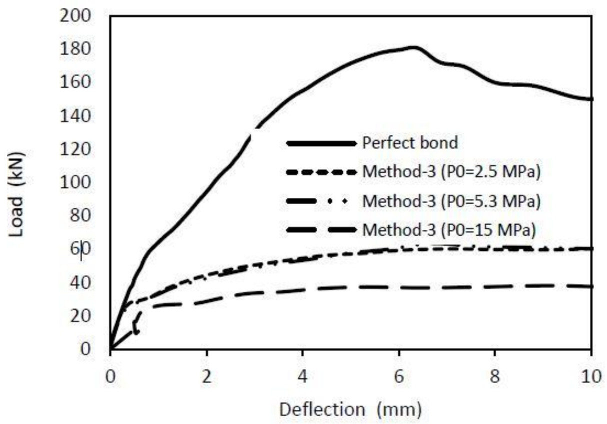

Fig. 14 Effects of changing P_0 value for Method-2 of bond modelling

comparing the results obtained through modeling based on surface-based contact and surface-based cohesive bond behaviors, as follows.

4.1.2 Surface-based contact bond case

The FE model for the same beam (NC-B2) was modified by replacing the perfect bond method with surface-based mechanical contact using Methods 1 and 2, as described in section 2.1.1. The load-deflection curves plotted using results of both methods, as shown in Fig. 13. The comparison of these two curves with the curve obtained using perfect bond method indicates that these two methods failed to simulate the bond behavior of non-corroded RC beams. The reason behind inability of these two method to simulate the bond behavior may be attributed to the fact that the friction alone in tangential behavior in these methods was not enough to develop good constraint especially if there is no additional applied pressure on steel bars to make the friction more effective.

In Method-3, the values of parameter μ (μ_s=1, μ_k=0.4, d_c=0.45) in Eq. (2) for the tangential behavior were taken from Amleh and Ghosh (2006) and $\dot{\gamma}_{eq}$ was calculated at each loading increment automatically by ABAQUS. For the normal behavior, pressure was used according to the Eq. (1), which was equal to 5.3 MPa, however, the resulting capacity was very small compared to perfect bond case (Fig. 14). Other normal pressure values were selected to capture the behavior of non-corroded RC beam. As shown in Fig. 14, even with the value of P_0 equal to 15 MPa, the capacity of the RC beam remained significantly lower than the actual capacity of beam. This is because at a larger value of P_0 there is early failure of concrete before development of the full strength of beam.

Therefore, it can be concluded that none of the three different methods based on surface contact bond were able to simulate the bond between the steel rebars and the surrounding concrete. Method-3 was used successfully by Amleh and Ghosh (2006) to simulate pullout tests but not for the behavior of beams and it was done using different analysis method (ABAQUS Standards).

4.1.3 Surface-based cohesive bond case

In order to model the rebars-concrete bond in ABAQUS by using the surface-based cohesive model, parameters that defines the cohesive interaction were defined carefully to reflect the actual behavior of the bond-slip relation between concrete and steel rebars. There are various models available in the literature for modelling the concrete-steel interface for corroded and non-corroded RC members. Many researchers used, with some modifications, the model proposed by Eligehausen *et al*. (1983) and prescribed by the Model Code 2010 (FIB 2010), Henriques *et al*. (2013), Ou and Nguyen (2014), Hanjari *et al*. (2011), Elbusaefi (2014).

Figs. 15 (a) and (b) show bond-slip model based on the Model Code 2010 and the approximation of bond model that is used in ABAQUS, respectively (Henriques *et al*. 2013). The approximation used in ABAQUS by expressions for the shear and normal stiffnesses are given as

$$k_{\mathrm{ss}} = k_{\mathrm{tt}} = \frac{\tau_{\max}}{S_1} \tag{15}$$

$$k_{\mathrm{nn}} = 100 k_{\mathrm{tt}} = 100 k_{\mathrm{tt}} \tag{16}$$

It is clear that the stiffness k_{nn} in the normal direction is assumed as fully rigid. Therefore, the value of k_{nn} is considered as an infinite stiffness according to assumption by Gan (2000).

Maaddawy *et al*. (2005) suggested Eq. (17) to estimate the bond stress $\tau_{\max}$ of non-corroded and corroded rebar in concrete (in MPa). It consists of two terms, the first is the influence from concrete, and the second is influence from stirrups. Eq. (17) was chosen in this study because it

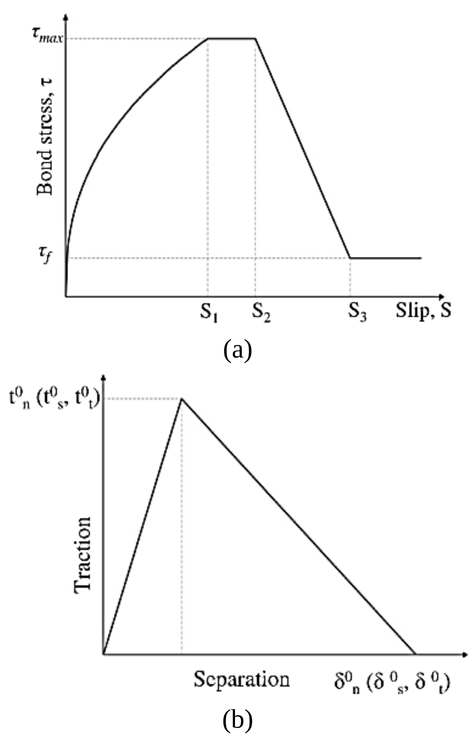

Fig. 15 (a) Bond-slip model in Model Code 2010 (b) Traction-Separation response available in ABAQUS (Henriques *et al*. 2013)

includes the effect of various parameters on the bond stress and it is valid for both corroded and non-corroded cases.

$$\tau_{\max} = R(0.55 + 0.24\frac{c_c}{d_b})\sqrt{f_c'} + 0.191\frac{A_t f_{\mathrm{yt}}}{S_s d_b} \tag{17}$$

where:

R =the bond loss reduction factor, it is equal to 1 for non-corroded case

c_c=smaller of concrete clear cover and one-half clear spacing between rebar

d_b=diameter of the rebar

S_s=spacing of the stirrup

A_t=total cross-sectional area of stirrup within S_s that crosses splitting planes

f_{yt}=yield stress of the stirrup.

Value of slip at maximum bond stress, S_1, is needed to compute stiffness values in Eq. (15). A model for slip values as proposed by Kallias and Imran Rafiq (2010) was adopted in this study. S_1 is equal to $S_{\max}$ given by Eq. (18) and maximum slip S_2=0.35 C_0, where C_0=rib spacing=half of the bar diameter (assumed). The used bond-slip relation is shown in Fig. 16 with dashed line indicating the bilinear approximation that is used in ABAQUS ($u_{\max}$ in Fig. 16 is the $\tau_{\max}$).

$$S_{\max} = 0.15 C_0 e^{\frac{10}{3}\ln\left(\frac{\tau_{\max}}{\tau_1}\right)} + S_0 \ln\left(\frac{\tau_1}{t_{\max}}\right) \tag{18}$$

where $\tau_1 = 2.57\sqrt{f_c'}$, and S_0 = 0.15 and 0.4 mm for plain and steel confined concrete, respectively.

Fig. 17 shows load-deflection curve using the above equations, with R=1 for the non-corroded beams, compared

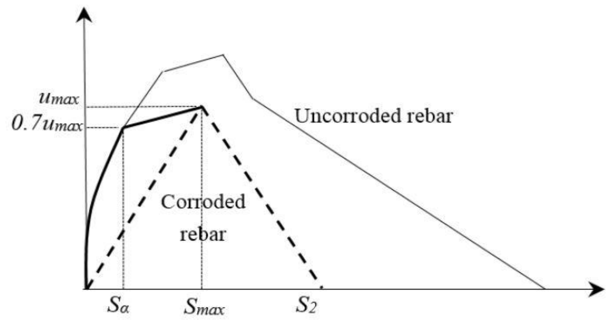

Fig. 16 Approximation of bond-slip (Kallias and Imran Rafiq 2010)

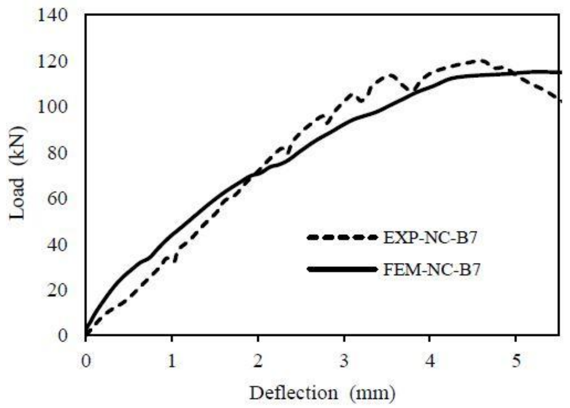

Fig. 17 Bond modeling by Surface-Based Cohesive vs. Perfect Bond (NC-B2)

with perfect bond case of beam NC-B2 (Lachemi *et al*. 2014). The result showed excellent agreement between the prefect bond case and cohesive bond model.

4.2 FE modeling for corroded beams

Since surface-based cohesive bond model was found to be most accurate for modeling the bond behavior of non-corroded beams, as mentioned in the previous section, this approach was adopted for the validation of the models for the corroded beams as well. To model the corroded beam, first FE is constructed assuming no corrosion as set forth in the prior sections. Suitable reduction of concrete and steel strength parameters and the bond between concrete and strength due to reinforcement corrosion is applied to simulate the corrosion effects.

a) Reduction in strength of concrete in the cover region

Reduction in the compressive strength of cracked concrete in the cover was determined using the following model (Coronelli and Gambarova 2004, Kallias and Imran Rafiq 2010, Hanjari *et al*. 2011, Ou and Nguyen 2014).

$$f_{cc}^{'} = \frac{f_c^{'}}{1 + k\frac{\varepsilon_1}{\varepsilon_c}} \tag{19}$$

In this work, k =0.1 for medium-diameter ribbed bars. ε_1 is a strain determined based on the corrosion crack width by the following expression

$$\varepsilon_1 = \frac{b_f - b_0}{b_0} = \frac{n_{\text{bar}}\, w_{\text{cr}}}{b_0} = \frac{n_{\text{bar}}\,[2\pi(v_{\text{cr}} - 1)x]}{b_0} \tag{20}$$

where: b_o=undamaged member section width; b_f=member width increased by corrosion cracking; n_{bar}=number of rebars in the compression zone; w_{cr}=crack width for a given corrosion penetration, x, and v_{cr}=ratio of volumetric expansion of the oxides with respect to the virgin material.

In this study, v_{cr}=2 was used as recommended by Hanjari *et al*. (2011) and many other researchers. After calculation of average cross-sectional area from the mass loss, corrosion penetration, x, of a corroded bar was determined by

$$x = \frac{D_0 - D_c}{2} \tag{21}$$

where: D_0 and D_c are the original and corroded bar diameters, respectively.

A reduction factor $\frac{f_{cC}^{'}}{f_c^{'}}$ is applied to take care of reduction in concrete tensile strength due to cracking.

b) Reduction in steel bar properties

It is well known that corrosion results into a reduction in the rebar's cross-sectional area, but this reduction in not uniform along the steel bar. It is reported that, as the corrosion increases, residual yield and ultimate forces, F_{yc} and F_{uc}, respectively, in corroded rebars decrease more rapidly than the average cross-sectional area, therefore, there is a reduction in yield stress f_{y} in addition to the decrease in the cross-sectional area (Du *et al*. 2005). This decrease is due to pitting corrosion, which causes stress concentration at pitting locations (Ou and Nguyen 2014). This is explained by Eq. (22)

$$\begin{aligned} f_{\text{yc}} &= \frac{F_{\text{yc}}}{A_s}(\text{with corrosion}) \;<\; f_{\text{y}} \\ &= \frac{F_{\text{y0}}}{A_{s0}}(\text{without corrosion}) \end{aligned} \tag{22}$$

Both, reductions in cross-sectional area and yield strength, can be combined by calculating the residual yield strength based on original non-corroded bar area (i.e, $f_{\text{yc}} = \frac{F_{\text{yc}}}{A_{s0}}$). In this study, the reduced yield strength, f_{yc}, and modulus of elasticity, E_{sc}, of corroded rebars were calculated using Eqs. (23) and (24) developed by (Al-Osta, 2013). This method of reduction enables the use of the same rebar 3D element for different degrees of corrosion.

$$f_{\text{yc}} = (1 - 0.011X_p)f_y \tag{23}$$

$$E_{\text{sc}} = (1 - 0.007X_p)E_s \tag{24}$$

where: X_P is is the loss of weight of reinforcing bar expressed as a percentage of original rebars weight (%).

Due to stress concentration at pitting locations, strain and stress are larger than those at other locations (Ou and Nguyen 2014). The residual ultimate strain of a corroded bar is computed using the empirical equation (Eq. (25)),

Table 5 A_1 and A_2 for Computation of Bond Reduction Factor (Maaddawy *et al*. 2005)

Corrosion current density, μA/cm^2	A_1	A_2
40	1.003	-0.037
90	1.104	-0.024
50	1.152	-0.021
250	1.163	-0.011
500	0.953	-0.014
1000	0.861	-0.014
2000	0.677	-0.009
4000	0.551	-0.01

proposed by Du *et al*. (2005).

$$\varepsilon_{\mathrm{uC}} = (1-\alpha_1 X_p)\varepsilon_{\mathrm{u0}} \tag{25}$$

Du *et al*. (2005) recommended α_1=0.03 for a bare bar and α_1= 0.05 for a bar embedded in concrete.

c) Reduction of bond strength

The proposed surface-based cohesive bond method depends on the values of maximum bond strength ($\tau_{\max}$), maximum bond slip (S_1), and bond stiffness (K_{ss}). In ABAQUS, the reduction in bond based on surface-based cohesion was simulated by reducing the, $\tau_{\max}$, which is the value of t_s for cohesive interaction. To reduce $\tau_{\max}$, values of reduction factor, *R*, in Eq. (17) were used. The *R* values were calculated using Eq. 26, given by Maaddawy *et al.* (2005).

$$R = \left(A_1 + A_2 X_p\right) \qquad (<\ 1) \tag{26}$$

The use of this reduction factor is advantageous as it depends on both mass loss (X_p) and variables A_1 and A_2. The values of A_1 and A_2, as given by Maaddawy *et al*. (2005) are presented in Table 5 for different corrosion current density levels.

S_1 and K_{ss} values were then modified according to Eqs. (15), (16), and (18) using the reduced value of $\tau_{\max}$ for corroded rebars instead of $\tau_{\max}$ of the non-corroded rebars.

4.2.1 Validation of the proposed FE models for corroded beams

4.2.1.1 Validation of flexural beams

a) Using Rodriguez et al. (1996) data

First beam used for validation was the control (un-corroded) beam specimen B-111. Then the models for two corroded beams (B113 and B115) were validated by considering the corrosion damages to sections of rebars, concrete cover, and bond between rebars and concrete, as described in section 4.2 using corrosion degrees (X_p) given in Table 3. The plots of the load-deflection data obtained from the FE models for non-corroded and corroded beams are compared with the plots of experimental load-deflection data, as shown in Fig. 18. It can be seen from Fig. 18 that a very good agreement exists between FE and experimental results for both the control (non-corroded) and the corroded beams (B111 and B113). The difference between the failure

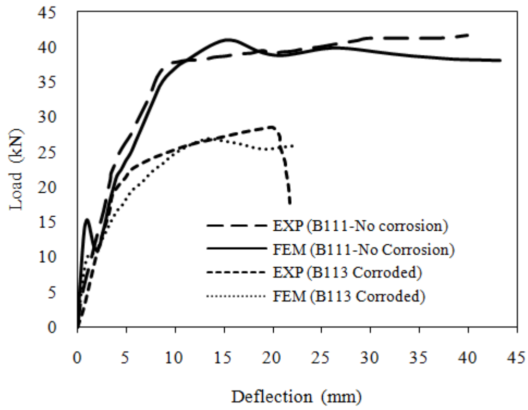

Fig. 18 Validation of FE models for B111 and B113

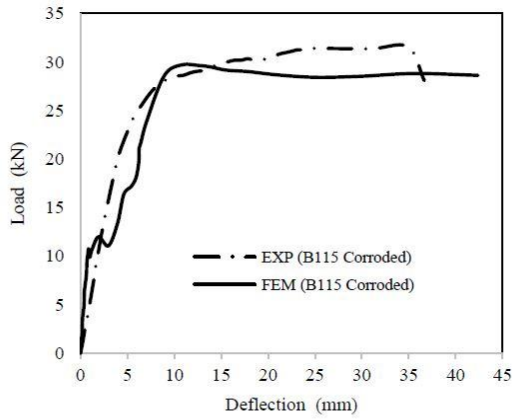

Fig. 19 Validation of FE model for corroded beam B-115

load obtained from the experimental work and FE model is less than 4%. For un-corroded beam, B111, the FE curve rises linearly until a load of 15 kN fallowed by a rapid drop. During this linear rise, deflection values of FE curve are the same as values obtained by linear deflection formula of simply supported beam. Load value drop is explained by first cracking of concrete when it reaches its modulus of rapture, f_r, and the beam section is no longer elastic. This cracking in concrete releases energy and causes decrease in load reaction value. However, the decrease is not sharp in B113 because the bottom cover is already week in tension by corrosion cracks. Additional successful validation was contacted using the corroded beam B115 as shown in Fig. 19.

b) Using Du et al. (2007) data

The load-deflection data reported by Du *et al*. (2007) after testing a partially corroded beam T282 was used in validating FE model developed for corroded beams. In this case, corrosion damage reductions were applied only to corroded bottom region. The plots of experimental data and the results of FE model are shown in Fig. 20. It can be seen from Fig. 20 that an excellent agreement of the model results and experimental data exists, in terms of both behavior and ultimate load capacity. This proves that the FE model presented in this study is also valid for beams with corrosion in specific zones.

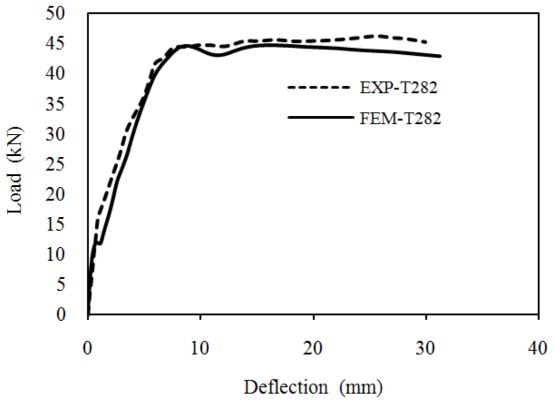

Fig. 20 Validation of FE model of corroded beam T282

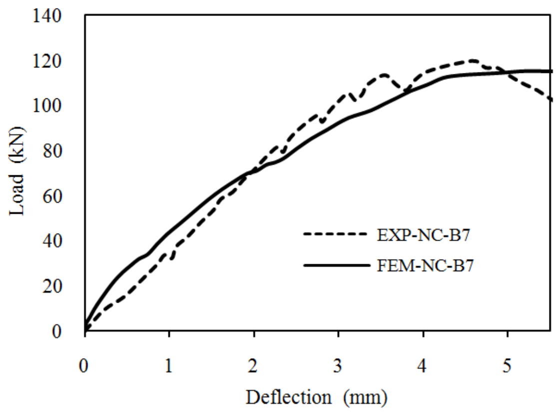

Fig. 21 Validation of the FE model for corroded shear-critical beam, NC-B7

4.2.1.2 Validation of shear beams

The proposed FE model was further validated for corroded short beams, which were designed to fail in shear. For this purpose, the experimental results of the shear-critical corroded beams NC-B7, prepared and tested by Lachemi *et al*. (2014) were used. This beam had a mass loss of an average 10.61% for both bottom bars and stirrups. The beam failure mode was controlled by shear. The strength of concrete in all cover regions due to corrosion were estimated based on the degree of corrosion from Eq. (19). The load-defection data recorded at the mid-span through experimental test and that obtained using the FE model are plotted in Fig. 21. In addition, shear failure was also confirmed in the ABAQUS FE model by damage pattern represented by d_t (Fig. 22). A difference of less than 5% was noted between the experimental and FE model's failure loads.

The results of another beam NC-B4 having a 14.62% of mass loss due corrosion and failed by shear cracks, as reported by Lachemi *et al*. (2014), were also used for validation of the FE model. The plots shown in Fig. 23 indicate a good agreement between FE model's and experimental results.

4.3 Parametric study

The parametric study was conducted to study the effects of key parameters, such as types of rebar corrosion damage,

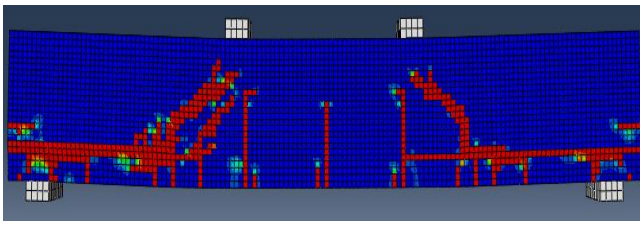

Fig. 22 Tension damage for FE model of NC-B7 beam

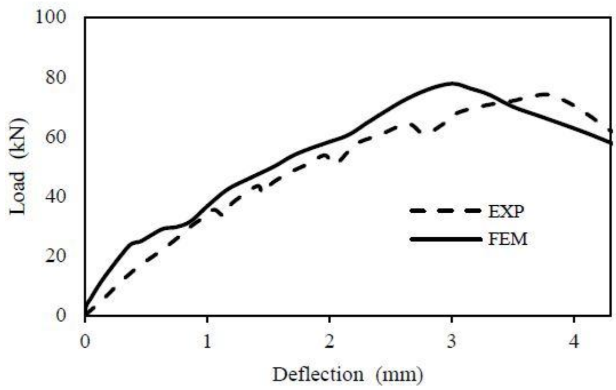

Fig. 23 Validation of FE model for corroded shear-critical beam (NC-B4)

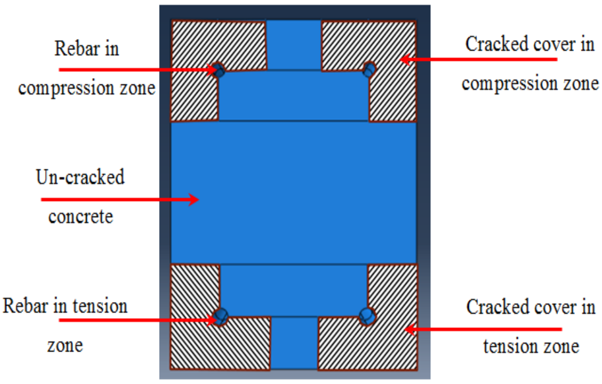

Fig. 24 Divided cross-section of beam for the parametric study

degree and location of rebar corrosion, on the behavior response and residual load carrying capacity of the corroded beams. The experimental data pertaining to beam B-113, reported by Rodriguez *et al*. (1996) and used earlier for validation of developed FE models, was used for the parametric study.

As recommended by Biondini and Vergani (2014), the areas adjacent to the corroded rebar, as indicated by hatched areas in Fig. 24, were considered as the zones of cracked concrete due to corrosion of rebars.

4.3.1 Type of rebar corrosion damages

FE simulations were conducted to study the effect of type of rebar corrosion damages on the failure load of corroded RC beam B-113. First, all types of rebar corrosion damages that included loss of bond, reduction in compressive strength due to cracked concrete, and reduction in material properties of steel were applied to the developed FE models and load-deflection results were obtained. Then,

Table 6 Residual strengths of steel and concrete around the corroded bar for different degrees of rebar corrosion

Beam	Degree of corrosion (mass loss %)	Residual strengths in the bottom zone (MPa)				Residual strengths in the top zone (MPa)			
		f_y steel (Eq. 23)	f_{cc} (cover concrete) (Eq. 19)	f_t (cover concrete) using reduction factor $=\frac{f'_{cc}}{f'_c}$	τ_{max} (Eq. 17)	f_y steel (Eq. 23)	f_{cc} (cover concrete) (Eq. 19)	f_t (cover concrete) using reduction factor $=\frac{f'_{cc}}{f'_c}$	τ_{max} (Eq. (17))
A-0	0	575.00	34.00	3.62	8.69	615.00	34.00	3.62	10.07
A-10	10	511.75	17.57	1.87	7.58	547.35	19.45	2.07	8.89
A-20	20	448.50	11.63	1.24	5.76	479.70	13.39	1.42	6.85
A-30	30	385.25	8.55	0.91	3.94	412.05	10.06	1.07	4.81
A-40	40	322.00	6.66	0.71	2.12	344.40	7.93	0.84	2.77
A-50	50	258.75	5.37	0.57	0.08	276.75	6.45	0.69	0.72

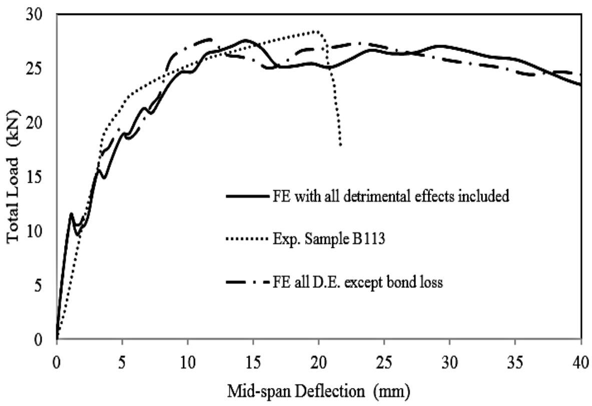

Fig. 25 Effect of bond loss in corroded beam B113

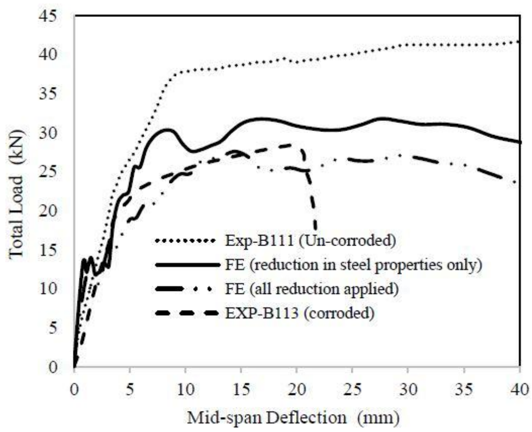

Fig. 26 Effect of reductions in steel properties of corroded beam B-113

in order to see the effect of not considering the bond damage, all types of corrosion damage parameters were considered in the FE models except the bond damage. Plots of the results predicted by FE models for beam B-113, with and without bond damage, are shown in Fig. 25 along with the plots of experimental data. It can be seen from Fig. 25 that the effect of bond loss is not critical for this particular beam because it has sufficient anchorage length at the ends. Similarly, the effect of steel damages (reductions in cross-sectional area, yield strength, and ductility of corroded rebar) alone on the behavior and failure load of corroded beam B-113 was studied. From the load-deflection curves in Fig. 26, it can be observed that the damage of steel properties had major effects on failure load of corroded beam (B113) as the effect of loss of bond was noted to be minimal for this beam. Further reduction in the load capacity when the effects of all types of corrosion damages are considered may be attributed to cracking of concrete in the compression zone.

4.3.2 Effect of degree of corrosion

In order to observe the effect of degree of rebar corrosion, several FE models with five different degree of corrosion in the range of 10 to 50% mass loss were considered for the beam (B-113). These corrosion degrees were considered to determine the losses of strengths of concrete and steel and loss of bond between steel and concrete in top and bottom zones of the beam. Table 6 shows the residual strengths of concrete and steel and loss of bond between steel and concrete, calculated for different degree of corrosion using Eqs. (17), (19), (23), and (24). The data presented in Table 6 were used to observe the effects of degree of corrosion using the developed FE models.

4.3.2.1 Effect of degree of corrosion in compression zone

Five FE models (denoted as AT-10, AT-20, AT-30, AT-40, and AT-50) were used to investigate the impact of degree of corrosion in top compression steel rebars using the residual properties as presented in Table 6. Plots of the load versus deflection data as shown in Fig. 27 indicate that no major change happened for the behavior and load capacity of the beam with corroded top bars (compression rebars) even with as high degree of corrosion as 40% mass loss. Small decrease in ultimate load, around 8%, and negligible change in stiffness is noted even at 50% degree of corrosion. These results are expected because of the fact that this beam is under-reinforced with ratio of steel in the tension zone=0.35×ρ_{max} that is less than the maximum ratio of steel ρ_{max} specified in ACI-318-14 (singly RC beam). Therefore, steel bars in compression region have negligible effect on the flexural capacity of the beam. The slight reduction in load capacity is only due to reduction of compressive strength for the cracked concrete in compressive zones.

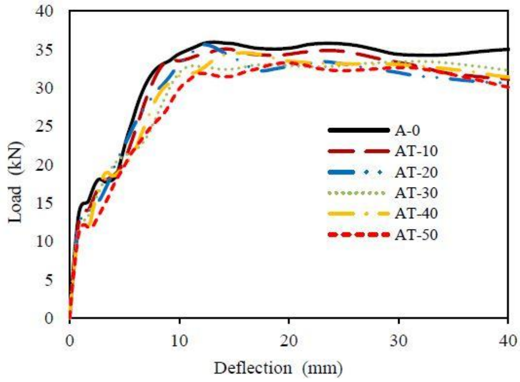

Fig. 27 Load vs. deflection for FE models with corroded top bars (compression rebars)

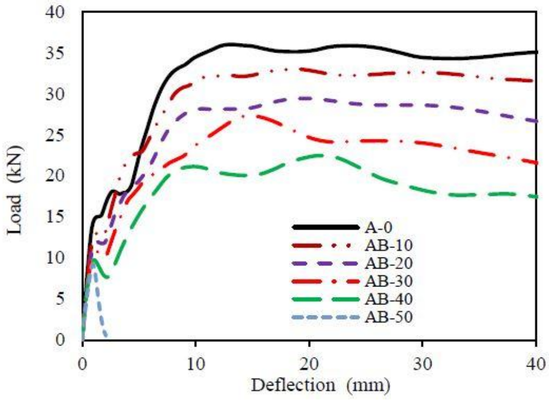

Fig. 28 Load-deflection curves for FE models with corrosions on bottom bars only

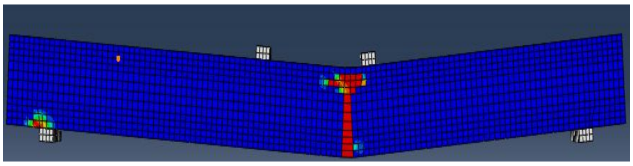

For beam corroded by 50% at bottom bars (AB-50)

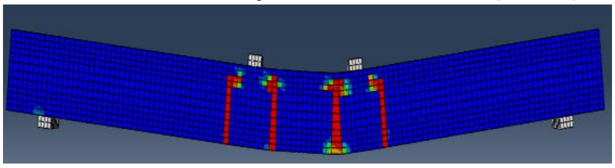

For beam corroded by 40% at bottom bars (AB-40)

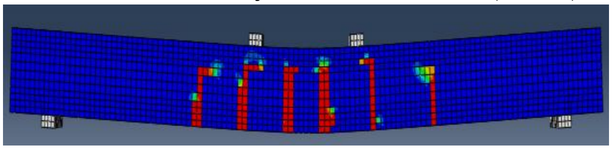

For un-corroded beam (A-0)

Fig. 29 Cracking patterns at different degrees of corrosion in the tension zone

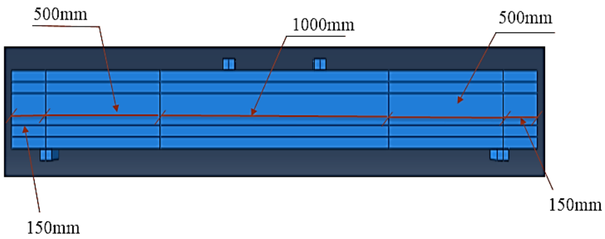

Fig. 30 Divided beam in the longitudinal direction for the parametric study

4.3.2.2 Effect of degree of corrosion in tension zone

Fig. 28 shows the plots of load versus deflection results obtained using FE models for the different degree of corrosion for the bottom bars (tension rebars). It can be observed from Fig. 28 that a uniform decreases in the load carrying capacity of the corroded beam occurs by increasing the corrosion degree up to 40%. Thereafter, with a degree of corrosion of 50%, the mode of failure the corroded beam changed from flexural failure to brittle failure due to heavy loss of bond with a negligible residual bond strength (τ_{max}=0.08 MPa). This brittle failure at high degree of corrosion is evident from the crack patterns shown in Fig. 29.

4.3.3 Effect of different locations of corrosion

The effect of applying corrosion on specific location along the longitudinal steel bars of the beam was studied. The beam with span of 2000 mm was divided into five segments along the longitudinal direction (one middle part of length 1000 mm, two side parts having length of 500 mm, and two small end parts with length of 150 mm), as shown in Fig. 30. Since corrosion in bottom bars is the critical for beam under consideration, two degrees of corrosion (40% and 50%) in the tension zone were considered for investigating the effect of changing the location of the corrosion. Details of locations of corrosion that were considered are given in Table 7.

First, results of three cases (MB-40, OSB-40, and TSB-40) were obtained using the FE models. The results from FE models (load versus deflection) are plotted in Fig. 31. It is observed that at 40% corrosion in the two sides did not decrease the load capacity in cases of OSB-40, and TSB-40 compared to the un-corroded beam. This may be attributed to the fact that there is enough bond strength (2.1 MPa) in the end segments having 150 mm length and the middle part has the full yield strength (575 MPa). On the other hand, dramatic drop in load carrying capacity occurred when applying the corrosion to middle part only as in MB-40 and its result is almost the same as applying the corrosion in the whole length.

The results from FE models (load versus deflection) are plotted in Fig. 32 for TSB-50, ASB-50, and MB-50 corresponding to 50% mass loss. Fig. 32 demonstrated that ASB-50 beam, which has un-corroded middle part, failed because of bond loss like AB-50 beam but after a little higher load. The beam TSB-50, which has corrosion in both segments with 500 mm length, does not undergo bond failure and has much higher load capacity than ASB-50. This is due to available enough bond strength within the end segments of length 150 mm to develop yield strength of rebars in the un-corroded middle part. To study the effect of steel-concrete bond in end segments of length 150 mm, FE model was used for the case M&S-B-50 by applying corrosion in the whole length of bottom bars except end zones and the result of load versus deflection is shown in

Table 7 Some FE models details used for studying effect of corrosion location

Beam notation	Degree of corrosion %	Location of applied corrosion	
		cross-section	longitudinal direction
AB-40	40%	both bottom bars	along the full length
AB-50	50%	both bottom bars	along the full length
AB-40-1	40%	one bottom bar	along the full length
MB-40	40%	both bottom bars	middle part only
TSB-40	40%	both bottom bars	in both 500 mm sides
OSB-40	40%	both bottom bars	in only one 500 mm side
TSB-40-1	40%	one bottom bar	in both 500 mm sides
ASB-50	50%	both bottom bars	in both sides and ends (only the middle part is not corroded)
M&S-B-50	50%	both bottom bars	in middle part and both sides (only the 150 mm ends are not corroded)

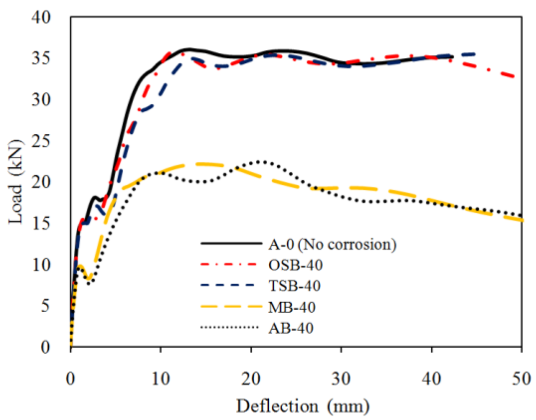

Fig. 31 Effect of changing the 40% corrosion along beam's long direction

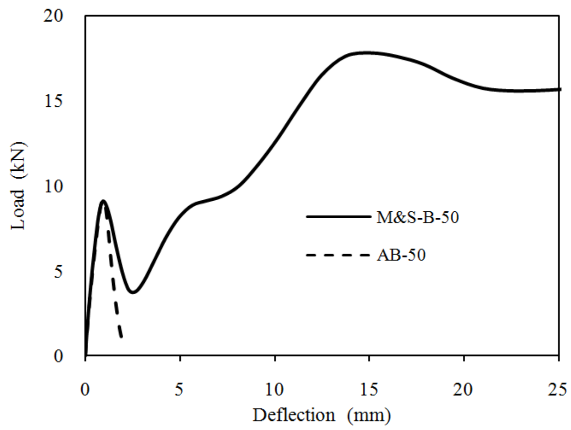

Fig. 33 Effect of un-corroded end zone in the beam

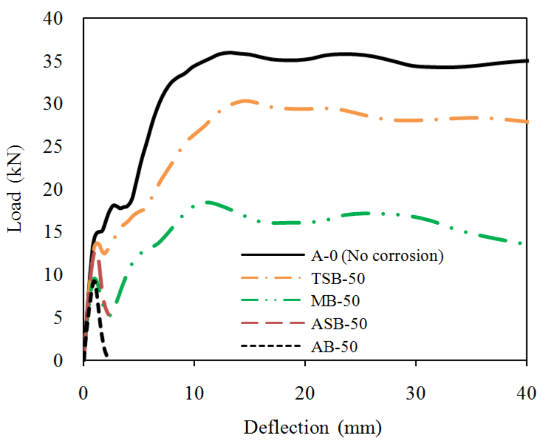

Fig. 32 Effect of changing the 50% corrosion along beam's long direction

Fig. 33. It is found that M&S-B-50 case achieved considerably higher capacity than AB-50.

5. Conclusions

A 3D finite element simulation for modeling corroded and non-corroded reinforced concrete beams was carried out. This nonlinear FE modeling used the explicit dynamic technique in ABAQUS and Concrete Damaged Plasticity model [CDP] mode for concrete. For the non-corroded beams, different surface interaction techniques were explored to simulate the bond between the 3D element steel bars and the surrounding concrete. That included perfect bond, mechanical contact using a variety of methods, and surface-based cohesive behavior. Validation of FE models using experimental data reported in literature showed that the surface-based cohesive behavior bond model exhibited most accurate results for both corroded and non-corroded beam cases.

The main conclusions may be summarized as follows:

• Damage-plasticity model for concrete in ABAQUS is found to model accurately the behavior of non-corroded and corroded RC beams.

• The proposed FEM for corroded RC beams was shown to predict not only the failure load but also the failure modes (flexural, shear, or bond failure) with a fair degree of accuracy and therefore, serves as an acceptable numerical tool to study the effect of different parameters on the behavior of beams with corroding reinforcement.

• Corrosion in top compression zone has very small effect on the behavior of flexural beams with small flexural reinforcement ratio (singly RC beam) even at very high degree of corrosion.

• In the corroded beam, the main sources for loss of flexural load capacity of beam is the loss of steel yield strength in tension reinforcement, which represents the reduction in rebars' cross-sectional area and pitting corrosion effect together.

• Small reduction in bond strength does not affect the behavior of long beams that have enough embedded length or rebars that are well anchored at their ends. However, the crack pattern depends on bond strength.
• The most critical corrosion-induced damage is the complete loss of bond between reinforcement and the concrete as it causes sudden failure and the beam acts as un-reinforced beam. In other words, substantial corrosion in zones of maximum bond stress is more critical than if it is in maximum moment zones.

Acknowledgments

The authors would like to acknowledge the support provided by the Deanship of Scientific Research (DSR) at King Fahd University of Petroleum & Minerals (KFUPM), Saudi Arabia for funding this work through Project No. JF141003. The support provided by the Department of Civil and Environmental Engineering is also acknowledged.

References

Abaqus Manual, A. (2013), Abaqus Analysis User's Manual version 6.13, Dassault Systèmes Simulia Corp., Providence, RI, USA.

ACI committee 318 (2014), Building Code Requirements for Structural Concrete and Commentary, ACI 318-14.

Almassri, B., Barros, J.A.O., Al Mahmoud, F. and Francois, R. (2015), "A FEM-based model to study the behaviour of corroded RC beams shear-repaired by NSM CFRP rods technique", *Compos. Struct.*, **131**, 731-741.

Almassri, B., Mahmoud, F.A. and Francois, R. (2016), "Behaviour of corroded reinforced concrete beams repaired with NSM CFRP rods, experimental and finite element study", *Compos. Part B: Eng.*, **92**, 477-488

Almusallam, A.A., Al-Gahtani, A.S. and Aziz, A.R. (1996), "Effect of reinforcement corrosion on bond strength", *Constr. Build. Mater.*, **10**(2), 123-129.

Al-Osta, M. (2013), "Reliability-based strength prediction model for corroded reinforced concrete columns and beam-columns", Ph.D Thesis, King Fahd University of Petroleum and Minerals, Dhahran, Saudi Arabia.

Amleh, L. and Ghosh, A. (2006), "Modeling the effect of corrosion on bond strength at the steel-concrete interface with finite-element analysis", *Can. J. Civil Eng.*, **33**(6), 673-682.

Bernard, S. (2013), "Finite element modelling of reinforced concrete beams with corroded shear reinforcement", MS Thesis, University of Ottawa, Ottawa, Canada.

Biondini, F. and Vergani, M. (2014), "Deteriorating beam finite element for nonlinear analysis of concrete structures under corrosion", *Struct. Infrastr. Eng.*, **11**(4), 519-532.

Birtel, V. and Mark, P. (2006), "Parameterised finite element modelling of RC beam shear failure", *2006 ABAQUS Users' Conference*. 95-108.

Bossio, A., Monetta, T., Belluccia, F., Lignolab, G.P. and Prota, A. (2015), "Modeling of concrete cracking due to corrosion process of reinforcement bars", *Cement Concrete Res.*, **71**, 78-92.

Chung, L., Cho, S.H., Kim, J.H. and Yi, S.T. (2004), "Correction factor suggestion for ACI development length provisions based on flexural testing of RC slabs with various levels of corroded reinforcing bars", *Eng. Struct.*, **26**(8), 1013-1026.

Coronelli, D. and Gambarova, P. (2004), "Structural assessment of corroded reinforced concrete beams: Modeling guidelines", *J. Struct. Eng.*, **130**(8), 1214-1224.

Dehestani, M. and Mousavi, S.S. (2015), "Modified steel bar model incorporating bond-slip effects for embedded element method", *Constr. Build. Mater.*, **81**, 284-290.

Du, Y., Clark, L.A. and Chan, A.H.C. (2005), "Effect of corrosion on ductility of reinforcing bars", *Mag. Concrete Res.*, **57**(7), 407-419.

Du, Y., Clark, L. and Chan, A.H.C. (2007), "Impact of reinforcement corrosion on ductile behavior of reinforced concrete beams", *ACI Struct. J.*, **104**, 285-293.

Elbusaefi, A.A. (2014), "The effect of steel bar corrosion on the bond strength of concrete manufactured with cement replacement materials", Ph.D Thesis, Cardiff University, Cardiff, Wales.

Eligehausen, R., Popov, E.P.E. and Bertero, V.V. (1983), "Local bond stress-slip relationships of deformed bars under generalized excitations", Rep. UCB/EERC-83/23 Earthquake Engineering Research Center, Univ.of California, Berkeley, CA.

FIB (2010), Model Code 2010 - First complete draft, **1**, fib Special Activity Group 5, New Model Code.

Gan, Y. (2000), "Bond stress and slip modeling in nonlinear finite element analysis of reinforced concrete structures", MS Thesis, University of Toronto, Toronto, Ontario, Canada

German, M. and Pamin, J. (2015), "FEM simulations of cracking in RC beams due to corrosion progress", *Arch. Civil Mech. Eng.*, **15**(4), 1160-1172

Hanjari, K.Z., Kettil, P. and Lundgren, K. (2011), "Analysis of mechanical behavior of corroded reinforced concrete structures", *ACI Struct. J.*, **108**(5), 532-541.

Henriques, J., Simões da Silva, L. and Valente, I.B. (2013), "Numerical modeling of composite beam to reinforced concrete wall joints Part I: Calibration of joint components", *Eng. Struct.*, **52**, 747-761.

Kallias, A.N. and Imran Rafiq, M. (2010), "Finite element investigation of the atructural eesponse of xorroded RC beams", *Eng. Struct.*, **32**(9), 2984-2994.

Lachemi, M., Al-Bayatia, N., Sahmaranb, M. and Anilb, O. (2014), "The effect of corrosion on shear behavior of reinforced self-consolidating concrete beams", *Eng. Struct.*, **79**, 1-12.

Lee, H.S., Noguchi, T. and Tomosawa, F. (2002), "Evaluation of the bond properties between concrete and reinforcement as a function of the degree of reinforcement corrosion", *Cement Concrete Res.*, **32**(8), 1313-1318.

Lee, J. and Fenves, G. (1998), "Plastic-damage model for cyclic loading of concrete structures", *J. Eng. Mech.*, **124**(8), 892-900.

Li, C.Q., Yang, S.T. and Saafi, M. (2014), "Numerical simulation of behavior of reinforced concrete structures considering corrosion effects on bonding", *J. Struct. Eng.*, **140(**12), 1-10.

Lubliner, J., Oliver, J., Oller, S. and Oñate, E. (1989), "A plastic-damage model for concrete", *Int. J. Solid. Struct.*, **25**(3), 299-326.

Maaddawy, E., Soudki, K. and Topper, T. (2005), "Analytical model to predict nonlinear flexural behavior of corroded reinforced concrete beams", *ACI Struct. J.*, **102**(4), 550-559.

Mander, J.B. (1983), "Seismic design of bridge piers", PhD Thesis, Dept. of Civil Engineering, Univ. of Canterbury, Christchurch, New Zealand.

Mangat, P.S. and Elgarf, M.S. (1999), "Bond characteristics of corroding reinforcement in concrete beams", *Mater. Struct.*, **32**, 89-97.

Mercan, B. (2011), "Modeling and behavior of prestressed concrete spandrel beams", Ph.D Thesis, University of Minnesota, Minneapolis and St. Paul, Minnesota.

Murcia-Delso, J. and Shing, P.B. (2015), "Bond-slip model for detailed finite-element analysis of reinforced concrete

structures", *J. Struct. Eng.*, **141**(4), 1-10.
Ou, Y.C. and Nguyen, N.D. (2014), "Plastic hinge length of corroded reinforced concrete beams", *ACI Struct. J.*, **111**(5), 1049-1057.
Potisuk, T., Higgins, C.C., Miller, T.H. and Yim, S.C. (2011), "Finite element analysis of reinforced concrete beams with corrosion subjected to shear", *Adv. Civil Eng.*, **2011**, 14.
Rodriguez, J., Ortega, L.M., Casal, J. and Diez, J.M. (1996), "Assessing structural conditions of concrete structures with corroded reinforcement", *Concrete Repair, Rehabilitation and Protection: proceedings of the international conference*, the University of Dundee, Scotland, UK.
Sánchez, P.J., Huespea, A.E., Oliverb, J. and Toroc, S. (2010), "Mesoscopic model to simulate the mechanical behavior of reinforced concrete members affected by corrosion", *Int. J. Solid. Struct.*, **47**(5), 559-570.
Simulia (2013), *Getting Started with Abaqus*, Keyword Edition,
Soh, C.K., Chiew, S.P. and Dong, Y.X. (1999), "Damage model for concrete-steel interface", *J. Eng. Mech.*, **125**(8), 979-983.
Stanish, K., Hooton, R.D. and Pantazopoulou, S.J. (1999), "Corrosion effects on bond strength in reinforced concrete", *Struct. J.*, **96**(6), 915-921.
Val, D.V and Chernin, L. (2009), "Serviceability reliability of reinforced concrete beams with corroded reinforcement", *J. Struct. Eng.*, **135**(8), 896-905.
Wenkenbach, I. (2011), "Tension stiffening in reinforced concrete members with large diameter reinforcement", MS Thesis, Durham University, Durham, England
Wu, Y. and Zhao, X. (2013), "Unified bond stress-slip model for reinforced concrete", *J. Struct. Eng.*, **139**(11), 1951-1962.
Xiaoming, Y. and Hongqiang, Z. (2012), "Finite element investigation on load carrying capacity of corroded RC beam based on bond-slip", *Jordan J. Civil Eng.*, **6**(1), 134-146.
Ziari, A. and Kianoush, M.R. (2014), "Finite-element parametric study of bond and splitting stresses in reinforced concrete tie members", *J. Struct. Eng.*, **140**(5), 04013106.

CC

Notations

A_t = total cross-sectional area of stirrup within S_s that crosses splitting planes
b_c and b_t = values between 0 and 1.
b_f = member width increased by corrosion cracking
b_o =undamaged member section width
C = thickness of concrete cover
C_0 = rib spacing (half of the bar diameter)
c_c = smaller of concrete clear cover and one-half clear spacing between rebar
d_b = diameter of the rebar
d_c = a user-defined decay coefficient
d_c and d_t = compression and tension damage parameters, respectively
D_0 and D_c = the original and corroded bar diameters, respectively
e = flow potential eccentricity
E = modulus of elasticity of concrete
E_{c1} = secant modulus of elasticity of concrete
E_s = modulus of elasticity of steel rebars
E_{sc} = modulus of elasticity of corroded rebars
f_{b0}/f_{c0} = Initial biaxial compressive stress to initial compressive stress
$f_{c'}$ = 28-day compressive strength of concrete
f'_{cc} = compressive strength of cracked concrete
f_{cm} = mean concrete cylinder compressive strength
f_t = modulus of rupture of concrete
f_y = yield strength of reinforcing rebars
f_{yt} = yield stress of the stirrup
f_{yc} = yield strength of corroded rebars
F_{yc} and F_{uc} =residual yield and ultimate forces, respectively
f_u = ultimate strength rebars
G_f =fracture energy
l_c = characteristic length
K = stiffness matrix
K_c = Ratio of second stress invariant on the tensile meridian
K_{nn}, K_{ss}, and K_{tt} = normal, shear and tangential stiffnesses, respectively
n_{bar} = number of rebars in the compression zone
P_o = pressure at zero clearance
P = normal contact pressure
R = the bond loss reduction factor, it is equal to 1 for non-corroded case
S_1 = Value of slip at maximum bond stress
S_{max} = maximum slip
S_s = spacing of the stirrup
t = traction
t_{max} = maximum bond strength
t_n^0, t_s^0 and t_t^0 = critical normal, shear and tangential stresses, respectively
X_p = corrosion mass loss
$\dot{\gamma}_{eq}$ = slip rate.
δ = separation or slip
δ_m = maximum slip in longitudinal tangential direction
ε_c = concrete compressive strain
ε_{c1} = concrete compressive strain at f_{cm}
ε_c^{pl} and ε_t^{pl} = plastic concrete compressive and tension strains, respectively
ε_{sh} = hardening strain of rebars
ε_{uc} = ultimate strain of corroded rebars
ε_{uo} = ultimate strain of non-corroded rebars
λ = viscosity parameter
k and η = two factors
v = Poisson's ratio of steel rebars
v_{cr} = ratio of volumetric expansion of the oxides with respect to the virgin material
μ = coefficient of friction
μ_s = static friction coefficient
μ_k = kinetic friction coefficient
ψ = Dilatation angle
σ_c = concrete stress
σ_c = concrete compressive stress
σ_t = concrete tension stress
τ_{crit} = critical shear stress
τ_{max} = bond stress between rebars and concrete
w_{cr} = crack width for a given corrosion penetration x
x = corrosion penetration